RSC Advances

This article can be cited before page numbers have been issued, to do this please use: S. Adhikari, R. Gupta, A. Surin, T. S. Kumar, S. Chakraborty, D. Sarkar and G. Madras, *RSC Adv.*, 2016, DOI: 10.1039/C6RA10472J.

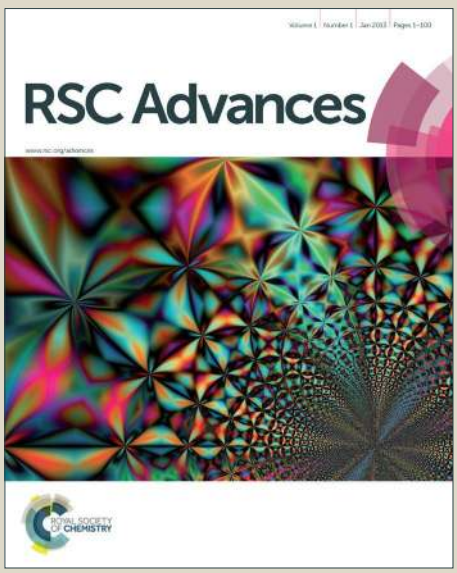

ROYAL SOCIETY OF CHEMISTRY

www.rsc.org/advances

View Article Online
DOI: 10.1039/C6RA10472J

Visible light assisted improved photocatalytic activity of combustion synthesized spongy-ZnO towards dye degradation and bacterial inactivation

Sangeeta Adhikari[1], Rimzhim Gupta[1], Angelica Surin[2], T. Satish Kumar[2], Subhabrata Chakraborty[2], Debasish Sarkar[2], Giridhar Madras[1]*

[1]Department of Chemical Engineering, Indian Institute of Science, Bangalore, India

[2]Department of Ceramic Engineering, National Institute of Technology, Rourkela, Orissa, India

View Article Online
DOI: 10.1039/C6RA10472J

Abstract

Spongy ZnO photocatalysts were succesfully synthesized by a simple, one-step solution combustion technique. The properties such as crystal structure, particle morphology and surface area were optimized through various processing parameters such as oxidizer to fuel ratio, combustion time and the temperature to control crystallinity, phase and yield. The stoichiometric oxidizer to fuel ratio was sufficient to develop porous and spongy-ZnO nanopowder with a high surface area of 32.6 m^2/g. The primary particle size of ZnO was found to be ~60 nm with a band gap of 2.92 eV. The photocatalytic activity of the spongy-ZnO photocatalyst was determined by degrading a model dye, crystal violet under visible light irradiation as well as natural solar light. Antibacterial study was also performed with *E.coli* as model microorganism under visible light. *E.coli* inactivation reaction order was found to be 1 and rate constant with ZnO was $13.11 \pm 0.4\ h^{-1}$. Spongy-ZnO maintains high photocatalytic activity under solar light irradiation in comparison to P-25 TiO_2. The catalytic efficiency was maintained for five cycles under visible light irradiation. Low electron-hole pair recombination with increased efficiency was observed under solar light due to strong absorption of photocatalyst under both UV and visible light. The main active species responsible for catalytic degradation are h^+ and •OH. The probable catalytic mechanism was proposed from the experimentally derived results. The effect of hydrogen peroxide on the photochemical reaction was also studied for dye degradation as well as bacterial inactivation.

Keywords: ZnO; Semiconductor; Sponge morphology; Photocatalyst; Dye Degradation, Antibacterial.

View Article Online
DOI: 10.1039/C6RA10472J

1. INTRODUCTION

A sustainable removal of wastes such as pathogens, organic dyes, and other water based pollutants from the environment is essential [1]. The present exploration reveals semiconductors as capable materials for photocatalytic oxidation to remove pollutants from water [2]. The major advantages of this process are the mild operating conditions, use of sunlight as a radiation source and the ease of operation [3]. ZnO is a wide band gap metal oxide semiconductor that finds uses in opto-electronics, sensors, and self-powered nanosystems [4]. Several studies have been carried out on the photoactivity of ZnO as its band gap (3.2 eV) is similar to TiO_2, but visible energy harvesting by ZnO makes it a superior candidate for photocatalysis [5]. However, its performance depends on the physical properties of the structures developed during the synthesis process [6]. Among the various wet chemical methods such as hydrothermal, solvothermal and sol-gel techniques used for ZnO synthesis, combustion synthesis has many advantages in terms of high yield, energy proficiency, cost effectiveness and easily tailored properties. The factors such as tedious processing, high difficulty in operation and long time consumption limit the usability of the former processes. However, solution combustion method is a simple, easy, one-step, makes use of low cost precursors, is environmental friendly, consumes low energy and does not require any sophisticated instruments [7]. The process takes place via self-propagation and is exothermic with the liberation of gases to produce highly porous structures [8].

Several researchers have used combustion method to synthesize ZnO nanostructures using different fuels and explored their optical, structural and other physical properties. ZnO nanoparticles were synthesized using oxalyldihydrazide as fuel and their structural and optical properties were explored [8]. Another fuel such as glycine was used with metallic zinc to synthesize ZnO nanostructures and different morphologies were obtained based on the synthesis parameters [9]. ZnO nanoparticles were synthesized by thermal decomposition of zinc acetate in the presence of an oleic acid as fuel [10]. Potti et al. studied the physical properties of mesoporous ZnO nanostructures synthesized using various fuels for photocatalytic degradation. The highest photoactivity for the

View Article Online
DOI: 10.1039/C6RA10472J

degradation of orange G degradation was achieved by ZnO nanocrystals [11] synthesized with oxalic acid. Ali et al. used ethylene glycol mixed with ethanol and zinc acetate as a source of zinc to produce flakes of ZnO nanoparticles and was used to degrade Rhodamine B [12]. ZnO is also known to inhibit the growth of both Gram negative and Gram positive bacteria. Its antimicrobial properties have extended its application in the fabrication of anti-microbial cotton fabrics and use in food packaging [13, 14]. Though, combustion synthesized ZnO has been potentially used in photocatalytic degradation of dye, there are very few reports on bacterial inactivation using combustion synthesized ZnO.

Citric acid is one of the efficient fuels to achieve highly porous crystalline nanostructures of materials such as TiO_2, ZnO, $La_{0.7}Sr_{0.3}Co_{0.5}Fe_{0.5}O_3$ (LSCF) and other materials [15-17]. However, citric acid has not been used as a fuel to synthesize ZnO. Other fuels such as oxalic acid and urea were also used to synthesize ZnO powders to understand the effect of fuels onto morphology and catalytic activity. In the current study, detailed processing experiments are carried using citric acid as a combustion fuel as the citric acid combusted ZnO imparts significant catalytic activity in comparison to powders synthesized by the other two fuels. Combustion synthesis of ZnO nanopowder using citric acid was optimized based on experimental parameters and characterized by physicochemical techniques. The photoactivity of the synthesized ZnO nanopowder was evaluated by degrading a dye (crystal violet) and inactivation of bacteria in order to determine their prospective environmental applications for the removal of organic contaminants and pathogens from wastewater.

2. EXPERIMENTAL SECTION

2.1. Material and methods

Analytical grade zinc nitrate hexahydrate ($Zn(NO_3)_2.6H_2O$) and citric acid ($C_6H_8O_7$) were purchased from Merck, India. Crystal Violet was purchased from SD Fine Chemicals. All of these chemicals were used without any further purification.

View Article Online
DOI: 10.1039/C6RA10472J

All the required accessories and materials for the bacterial experiments such as pipette tips, Eppendorf tubes and sterile centrifuge tubes were purchased from Tarsons, India. Nutrient agar and Luria-Bertani broth were supplied by HiMedia, India. Sterile Petri dishes were supplied by Genexy's, India.

2.2. Preparation of Spongy ZnO photocatalyst

In the typical synthesis process, stoichiometric amounts of oxidizer zinc nitrate hexahydrate and fuel citric acid were taken in a beaker and dissolved in 2 ml of deionized water. The beaker containing the solution was magnetically stirred for about 20 min to achieve homogeneous mixing. The stoichiometric reaction is given in Equation 1. The mixture was then kept in a preheated muffle furnace at 400 ± 10^{o}C for combustion. After combustion, the beaker was cooled to room temperature. A porous mass of powder was collected from inside the beaker. The optimization of the crystal structure and morphology was carried out by varying the oxidizer to fuel ratio (4/9, 5/9 (stoichiometric) and 6/9), time and temperature of combustion. A series of combustion synthesis experiments were conducted based on the above parameters and the powders were characterized by different physicochemical techniques to achieve optimal conditions. Similarly, stoichiometric amount of oxidizer and other fuels (oxalic acid and urea) were taken for combustion synthesis of ZnO nanopowder for comparative studies.

$$Zn(NO_3)_2.6H_2O + \frac{5}{9} C_6H_{10}O_8 \rightarrow ZnO + N_2 + \frac{10}{3} CO_2 + \frac{79}{9} H_2O \quad (1)$$

2.3. Photochemical reactor for antibacterial experiments

Batch process was followed to carry out the visible light experiments. A metal halide lamp of 400 W was placed inside a quartz jacket whose inlet was connected to continuous water chiller to reduce the temperature and remove the dissipated heat so as to maintain a constant temperature for the reaction. The UV content from the metal halide lamp was cut off using glass beaker as batch reactor. A 30 mL bacterial solution was taken for all the antibacterial experiments. The initial cell concentration was maintained at ~10^8 CFU/mL. The intensity of the metal halide lamp was observed to be 42,800 lux.

View Article Online
DOI: 10.1039/C6RA10472J

2.4. Culture and microorganism growth

Antibacterial experiments were carried out with *E.coli* strain MG1655 as a model bacterium. Glycerol stock stored at -80 °C was used to prepare the inoculum. Bacteria was grown in sterile Luria-Bertani broth. 100 µL inoculum was taken in 300 ml of broth and kept in shaking incubator (Orbitek, India) at 170 rpm and 37 °C. 100 µL of glycerol stock was poured into 2 % liquid media for overnight growth of bacterium, in order to prepare mother culture. 100 µL of mother culture was inoculated in 2 % media and allowed to grow for 6 h to prepare bacterial culture for reaction. Plating was carried with 100 µL of diluted samples on 2.8 % solidified nutrient agar. Enumeration of colonies was performed to observe the degradation of the *E.coli*.

2.5. Catalyst Characterization

The powder X-ray diffraction (XRD) patterns were recorded for all the synthesized materials under different conditions using a Philips X-Ray diffractometer with Ni filtered Cu-Kα radiation (λ= 0.15418 nm). The structural analyses of the selected samples were carried by Thermo Scientific iS10 Nicolet FT-IR spectrophotometer. The pressed pellets prepared using KBr powder were used as specimens, and each spectrum was recorded in the wavenumber range 400-4000 cm^{-1}. Field-emission scanning electron microscopy (FESEM) measurements were performed for the optimized ZnO particles using NOVA NANOSEM FEI 450 system. The measurement was carried by mounting the powder on a carbon tape attached to an SEM stub followed by sputter coating of gold onto the powder for 2 min. The morphology of the ZnO particles was further characterized by JEOL JEM-2100 Transmission electron microscopy (TEM). Specific BET surface area of the optimized powders was measured in the presence of nitrogen adsorbate in a Quantachrome Autosorb BET apparatus, USA. Shimadzu spectrophotometer UV-2450 was used to carry out the UV-DRS measurement to evaluate the band gap energy of ZnO nanoparticles in the wavelength of 200 – 800 nm.The reference used was barium sulphate. Photoluminescence measurement of spongy-ZnO nanopowder was carrried using Hitachi F-4500 spectrofluorimeter.

View Article Online
DOI: 10.1039/C6RA10472J

2.6. Photocatalytic Experiments

2.6.1. Experimental procedure for dye degradation

The photocatalytic activity of synthesized ZnO was evaluated both in the presence of visible light and natural sunlight by using crystal violet (CV) as a typical dye pollutant.The standard stock solution of crystal violet was prepared having concentration of 20 mg/L, which was maintained for all the catalytic experiments. In the typical procedure, 50 ml of CV dye solution with 50 mg ZnO nanopowder catalyst was taken into a Pyrex reactor and the suspension was magnetically stirred during the photochemical reaction under light irradiation. The visible light irradiation experiment was carried using the light source given in section 2.3. All the sunlight experiments were carried out between 12 pm to 2 pm as the fluctuations of solar intensity are minimal in this duration. The solar intensity variation was recorded using Eppley PSP 32483F3 radiometer, Newport, USA. The average solar intensity observed was 0.768 kW m^{-2}. Prior to the reaction, the suspension was allowed to reach adsorption desorption equilibrium in dark. Few ml of aliquots were sampled after certain intervals and centrifuged to separate the catalyst from the solution. The concentration of crystal violet was determined by UV absorbance. A standard curve of absorbance and concentration was constructed based on UV absorbance at λ_{max} of 590 nm. In order to determine formation of other intermediates, the samples were scanned over the complete UV-Vis range of 200-800 nm. No extra peaks other than peak at 590 nm was observed initially or during the course of degradation. This indicates no intermediates were formed. In order to further quantify the degradation, TOC analysis was carried out with a shimadzu-70C-VCSN analyzer. Therefore, mineralization could be calculated. The reuse of the catalyst was also carried to understand the stability of the catalyst upon consecutive recycling. After each experiment, the catalyst was separated by centrifugation followed by washing and finally dried for another photochemical experiment. Experiments in the presence of different scavengers were carried out to understand the photochemical mechanism. Each experiment was carried out thrice and the experimental error was less than ± 3% in the % degradation reported.

View Article Online
DOI: 10.1039/C6RA10472J

2.6.2. Experimental procedure for antibacterial study

In order to ensure the contaminant free environment, sterilization of all the required accessories such as glasswares, micro pipette tips, Eppendorf tubes, nutrient agar, Luria-Bertani broth, DI Millipore water was autoclaved at 121 °C for 90 min. 30 mL of freshly prepared culture was centrifuged at 4000 rpm for 5 min. The suspended pellet was washed twice with sterile DI water. Later, the pellet was re-suspended in sterile DI water of volume 30 mL. This bacterial solution containing 0.25 g/L catalyst loading was directly used for the experiment. Experiment was performed for 1 h and samples were collected after every 20 min interval. The collected samples were diluted in 900 µL of sterile water upto appropriate dilution (~ 30-300 CFU/mL). 100 µL of the diluted sample was spread uniformly on the agar plates. After incubation at 37^{o}C, the colonies were measured with a blank agar plate was kept as a control to detect any contamination either in incubator/ laminar hood. 2, 10, 100, 250 and 500 mM H_2O_2 were added to monitor the enhancement in photodegradation of *E.coli* bacterium.

Photocatalysis experiments were done in presence of light and catalyst. Parameters such as temperature, pH, irradiation intensity, rotation per minute and catalyst loading were kept constant for all the experiments. Experiments were conducted for 1 h in the presence of catalyst but without any light. This was to ensure adsorption-desorption equilibrium was reached. These are referred as dark experiments. Similarly, experiments were conducted with light in the absence of any catalyst. These photolysis experiments are also reported and compared with the catalytic experiments. The effect of combustion synthesised ZnO was observed and the results were compared with Degussa P-25 TiO_2. 200 µL of H_2O_2 was added to see the accelerated effect of externally provided ROS radicals on degradation of bacteria.

View Article Online
DOI: 10.1039/C6RA10472J

3. RESULTS AND DISCUSSION

3.1. Structural Characterization of spongy-ZnO photocatalyst

The X-ray diffraction patterns of the synthesized ZnO powders are shown in Figure 1. The designing of the experiments was made to understand the crystal structure and crystallinity of the powders under different parameters such as oxidizer by fuel ratio, combustion time, and temperature. Figure 1a illustrates the effect of oxidizer to fuel ratio for stoichiometric, fuel excess and deficient condition under constant parameters of 400^{o}C and 40 min. It is observed that all the XRD patterns correspond to the hexagonal wurtzite crystal structure matching well with JCPDS No 79-0206 having space group P63mc with peaks indexed to (100), (002), (101), (102), (110), (103), (200) and (112), respectively. The fuel deficient (O/F = 4/9) condition shows an additional peak along with the hexagonal phase that can be associated with the oxidizer, zinc nitrate hexahydrate (JCPDS: 46-0593). This suggests that the combustion of the oxidizer is incomplete at lower fuel content. Though, stoichiometric oxidizer to fuel ratio (O/F = 5/9) and fuel excess (O/F = 6/9) shows hexagonal phases, there is a difference in crystallinity in both the XRD patterns. The calculated crystallite sizes are 25 nm, 29 nm and 44 nm for fuel deficient, stoichiometric and fuel excess, respectively. The specific surface areas of fuel excess and stoichiometric are 25.8 m^2/g and 32.6 m^2/g, respectively. The excess fuel content leads to vigorous combustion and produces powders with high crystallinity having a lower surface area in comparison to the stoichiometric condition. Thus, further experiments have been carried using the stoichiometric oxidizer to fuel ratio. The surface area depends on the growth kinetics of the particles. Therefore, particles have been synthesized at 400^{o}C upon varying the time, as shown in Figure 1b. All the XRD patterns are found to be identical and matching with hexagonal crystal structure but the powders synthesized at 40 min have optimum crystallinity without compromising the surface area. This is due to uniform particle size, which is confirmed later using imaging method.

In every combustion reaction, the combustion temperature depends on the decomposition temperature of the fuel. The auto-ignition temperature of citric acid is ~350 ^{o}C. The combustion temperature was varied from 300-450 ^{o}C taking stoichiometric reactants for a constant duration of 40

View Article Online
DOI: 10.1039/C6RA10472J

min, as shown in Figure 1c. The growth of the primary peaks of the hexagonal phase has been observed till 350°C. However, beyond 350°C, there is no change in the XRD patterns, which is further supported by the analysis of functional groups. The above results suggest that the combustion of stoichiometric oxidizer to fuel ratio at 400 °C for 40 min produces a high yield of ZnO nanoparticles. A composite XRD pattern for combustion synthesized ZnO powders as an effect of different fuels (stoichiometric reaction) has been shown in Figure 1d. All the XRD patterns correlate well with the hexagonal wurtzite crystal structure of ZnO. The morphological analysis for these powders has been explored in later section.

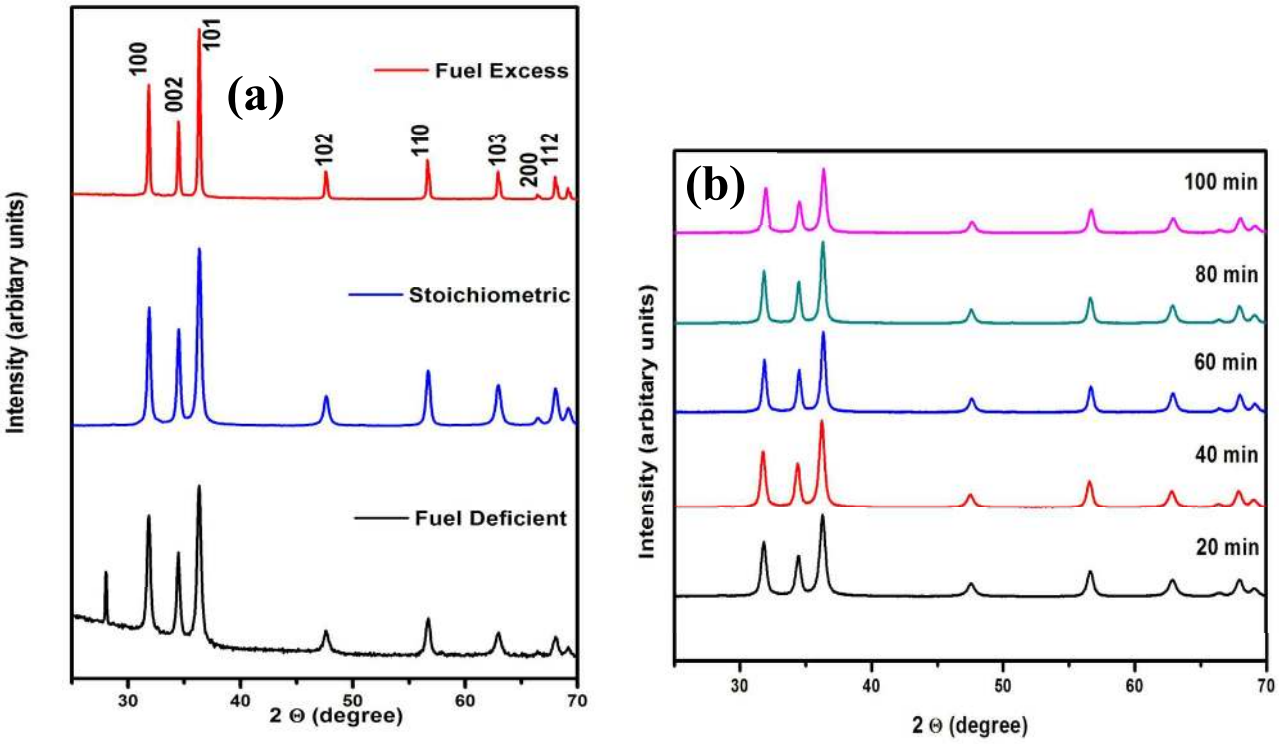

View Article Online
DOI: 10.1039/C6RA10472J

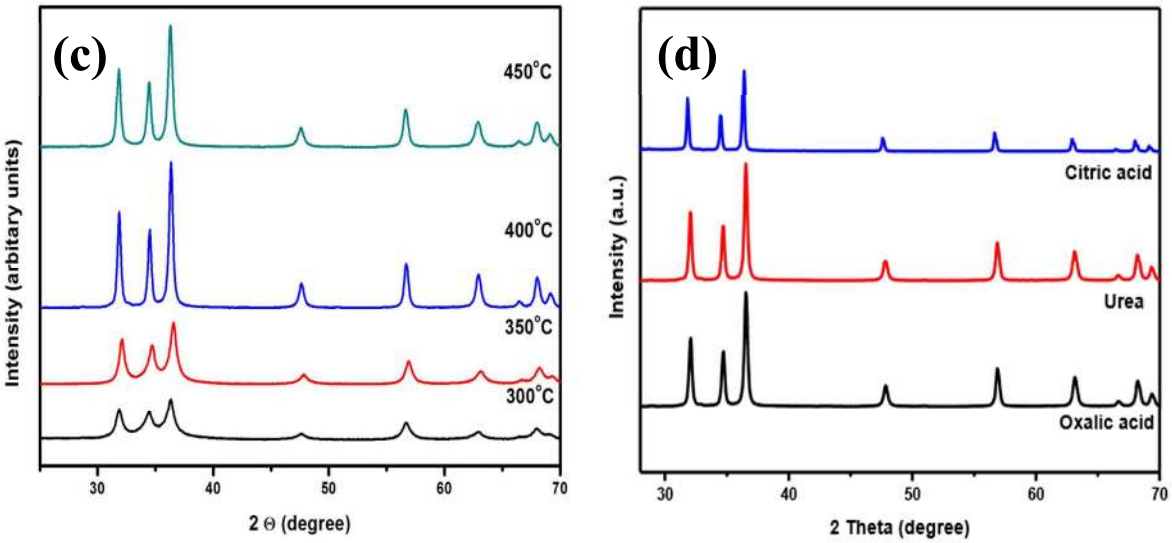

Figure 1: Composite XRD patterns: (a) Effect of Oxidizer/Fuel ratio, (b) Effect of Time, (c) Effect of Temperature and (d) Effect of fuels under stoichiometry.

3.2. Vibrational spectra analysis

The phase formation with the presence of functional groups under different synthesis condition has been carried using FT-IR spectroscopy. Figure 2 shows the FT-IR spectra for ZnO powders obtained under conditions: stoichiometric oxidizer to fuel ratio at 400°C for 40 min (optimized condition); fuel deficient at 400°C for 40 min (lower fuel condition) and stoichiometric ratio at 350°C for 40 min (lower temperature condition). Identical vibrational peak has been observed for all the conditions at 532 cm^{-1} that corresponds to Zn-O vibrations. The pure form of ZnO powders obtained under optimized condition has no other functional groups. There is a broad absorption peak and a sharp peak observed at 3300 cm^{-1} and 2920 cm^{-1}, respectively, that can be attributed to the vibrations from O-H group. This corresponds to the presence of water molecule either physically or chemically adsorbed onto the powder surface. The peaks in the wavenumber range of 1250 cm^{-1} to 1750 cm^{-1} are due to asymmetric and symmetric stretching of N-O groups [18]. Hence, FT-IR spectroscopy confirms that some functional groups like NO and OH are obtained that correspond to partial combustion during the reaction [19].

View Article Online
DOI: 10.1039/C6RA10472J

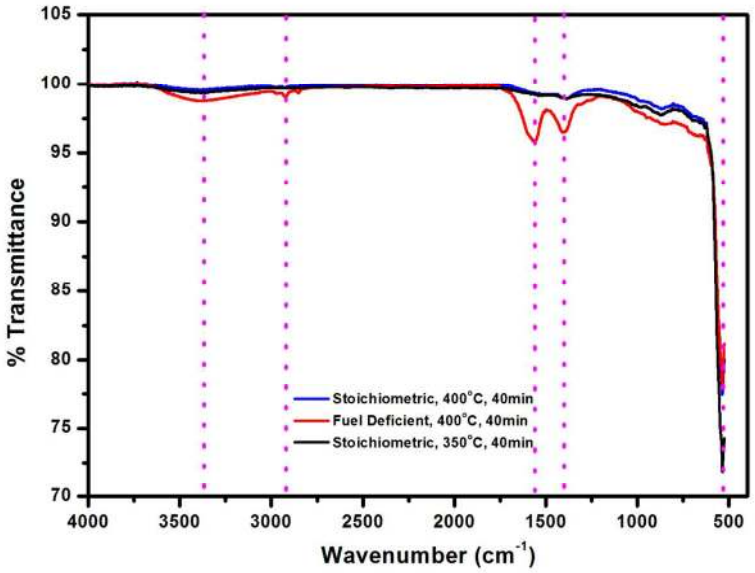

Figure 2: FTIR-Spectrum of ZnO nanopowders under different conditions.

3.3. Morphological analysis

The morphology, particle sizes and nature of the powders were investigated in detail using FE-SEM and TEM as shown in Figure 3 and Figure 4, respectively. Figure 3a and Figure 3b shows the low resolution and high resolution FE-SEM micrographs of the optimized ZnO powders. The low resolution image shows the porous nature of ZnO powders and appears as sponge-like rose structure.

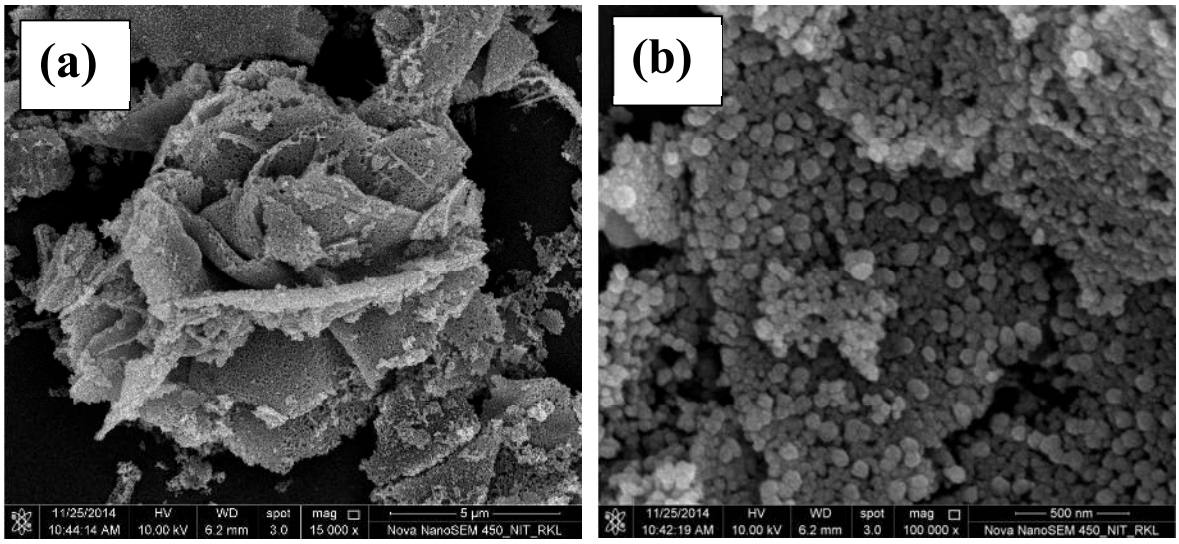

Figure 3: FESEM images of optimized ZnO nanopowders.

View Article Online
DOI: 10.1039/C6RA10472J

The oriented growth of particles is difficult during the combustion process as the reaction is highly rapid and exothermic in nature. However, this rapid process allows easy burn out of carbonaceous matter to achieve better porosity. The fluffy or spongy nature of the powder is due to rapid diffusion of heat as the reaction releases a large amount of gases [20]. The high resolution image (Figure 3b) shows that the sponge-like structure constitutes of near spherical particles having average primary particle size ~60 nm. High agglomeration of primary particles with an uneven distribution of particle sizes is also observed. The pores in the structure are clearly visible as the particles are accumulated to form secondary particles.

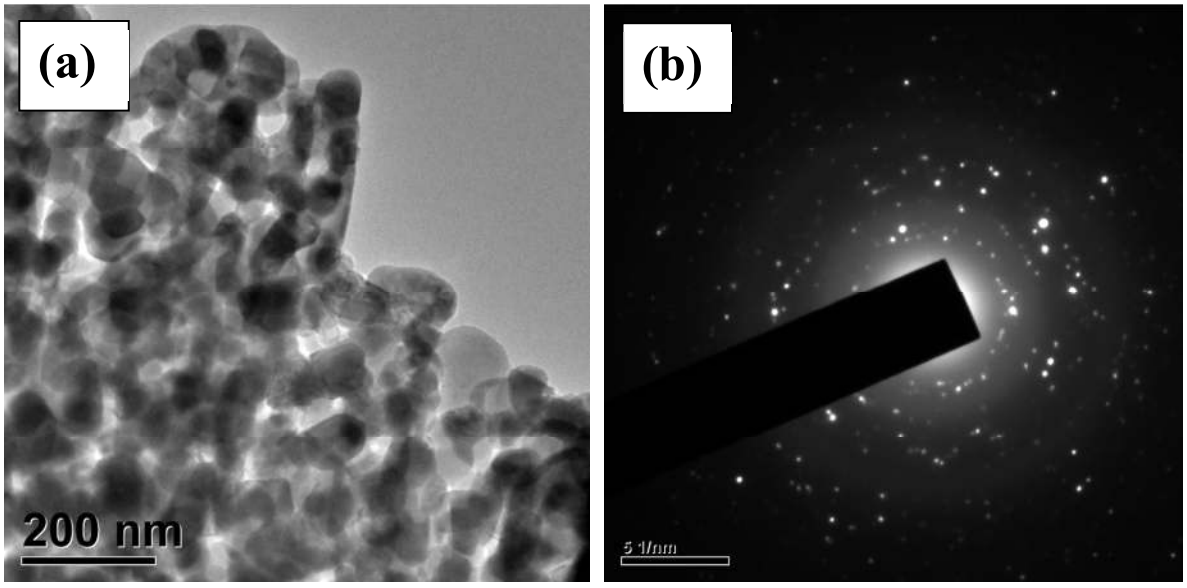

Figure 4: TEM images of optimized ZnO nanopowders.

Morphological characteristics of the sponge-ZnO can be better understood using TEM technique. TEM micrograph and Selected Area Electron Diffraction (SAED) pattern of the sponge-ZnO has been shown in Figure 4a and Figure 4b, respectively. TEM micrograph shows that the near spherical particles are aggregated similarly as shown in FESEM image. SAED pattern shows the formation of concentric circles due to the accumulation of nanoparticles that confirms particles to have a high crystalline nature. The above result suggests the formation of porous spongy-ZnO nanopowders by solution-combustion route.

View Article Online
DOI: 10.1039/C6RA10472J

The FESEM images of ZnO powders synthesized using oxalic acid and urea were found to have quasi-fiber and flake like structures as shown in Figure 5a and Figure 5b. Quasi-fiber structure was found to have length ~2.9 μm and width ~0.5 μm, respectively whereas flake like structures have length ~1.2 μm and thickness ~80 nm. The flake-like particles seem to have mixed with other primary spherical particles agglomerated to form bigger secondary particles. The specific surface area observed for quasi-fiber and flake particles were found to be 17.8 and 10.9 m^2/g which is very less in comparison to spongy-ZnO that is 32.6 m^2/g.

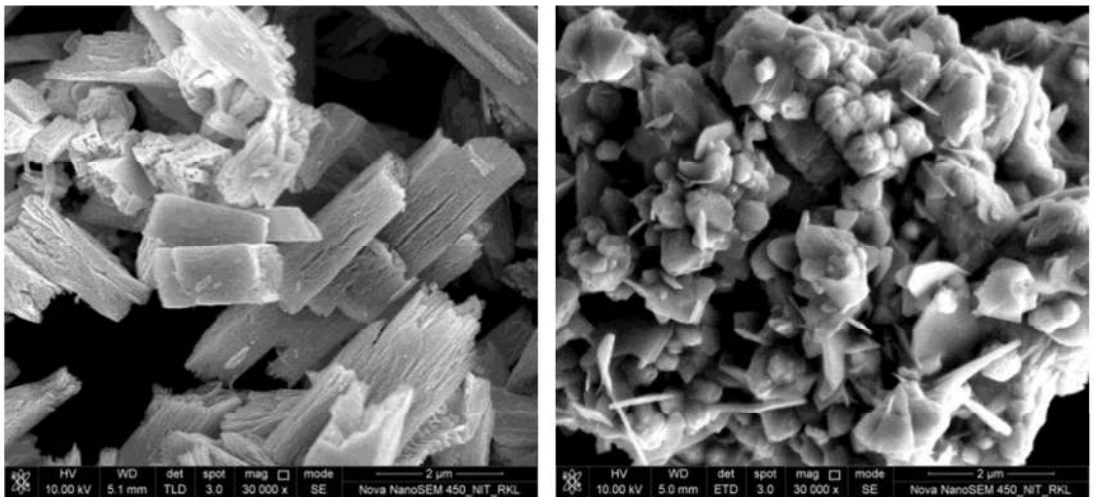

Figure 5. FESEM images of ZnO synthesized by fuel (a) Oxalic acid and (b) Urea.

3.4. Optical Absorption of Spongy-ZnO photocatalyst

The UV-Vis diffuse reflectance spectrum of optimized porous spongy-ZnO nanopowder is shown in Figure 6. The reflectance spectrum is converted to Kubelka-Munk absorption spectra using the function: $KMU = (1-R)^2/2R$, where R represents the reflectance data. The inset in the figure is the Tauc plot, which is used to calculate the band gap energy. The plot is $(KMU*h\upsilon)^{1/2}$ versus photon energy ($h\upsilon$) where the linear extrapolation to the photon energy gives the band gap of the material. The calculated band gap is 2.92 eV. The decrease in the band gap energy is probably due to the red shift of the absorption edge from UV to near visible region. Another probable reason could be vacancy of oxygen in the lattice of ZnO resulting from rapid exothermic combustion process [21, 22].

View Article Online
DOI: 10.1039/C6RA10472J

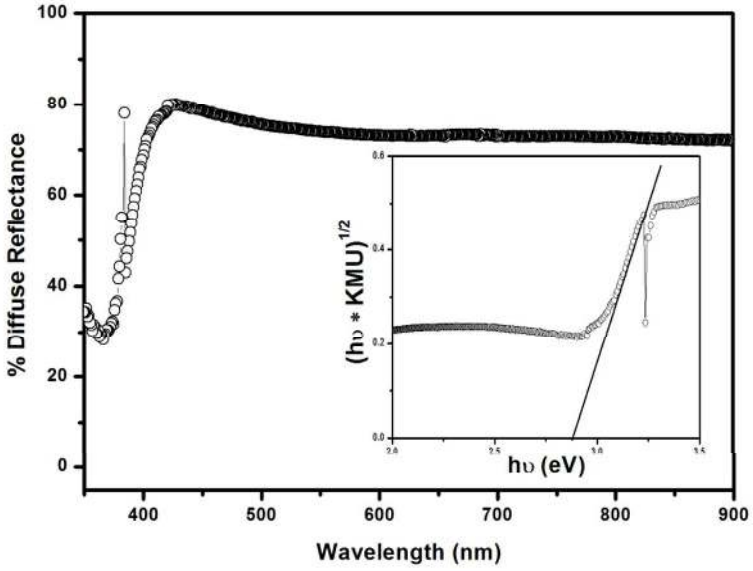

Figure 6: UV-Vis Diffuse Reflectance spectra of spongy-ZnO nanopowders.

3.5. Photoluminescence study

Photoluminescence (PL) spectra of all the three ZnO nanopowders have been analyzed to better understand the functioning of photocatalysts, as shown in Figure 7. Each of the PL spectra show emission at both UV and visible region when excited at 350 nm. The UV emission at 395 nm is associated with the recombination of electron and hole in the conduction and valence band, respectively [23]. This peak is nearly constant for all the three ZnO PL spectra. It can be observed that the blue–green emissions in the range of 450 to 550 nm show a distinct shift in the emission energies. As the structure becomes anisotropically porous, the peak shifts to higher wavelength energy. The weak emission at 410 nm in PL spectra can be attributed to the exciton transition. This violet emission takes place as a result of electron transition from a low donor level of neutral zinc interstitial (Zn_i) to the top of the valence band. Another probable reason could be the transition to interstitial oxygen level (O_i) from the base of conduction band (CB) [24]. The peak in the visible region at 482 nm for citric acid assisted synthesized ZnO catalyst corresponds to the blue emission that can be attributed to the electronic transition between shallow donor and deep acceptor. Thus, it is associated with the intrinsic defects such as Zn interstitials or oxygen vacancies and their structural complexes in nanostructures of ZnO. In the present case, the broad emission in the visible region suggests decreased density of

View Article Online
DOI: 10.1039/C6RA10472J

surface defect states. A broad green emission at 525 nm can be attributed to the vacancy from singly ionized oxygen in ZnO resulting from the radiative recombination of photogenerated hole relating in the single ionized charge state of this defect. The resultant emissions observed are due to electron-hole recombination from the localized states with energy levels cavernously positioned in the band gap producing lower energy emissions. Vacant oxygen sites are the most common defects that act as radiative centers in the luminescence processes [25]. The radiative recombination is the least for ZnO catalyst synthesized using citric acid in comparison to other fuel synthesized ZnO.

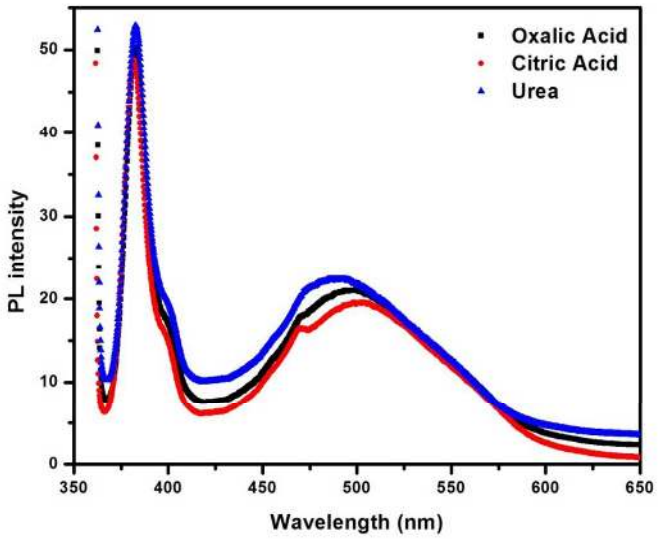

Figure 7: Composite photoluminescence spectra of ZnO nanopowders synthesized using different fuels.

3.6. Photocatalytic Activity

In the present study, ZnO powders have been prepared easily by one step solution combustion method using different fuels. Crystal Violet (CV, $C_{25}N_3H_{30}Cl$) is a typical organic dye pollutant. Thus, CV has been taken as a representative dye pollutant for evaluation of the photocatalytic performance of ZnO powders. Initially, photocatalytic experiments were carried to understand the effect of ZnO morphology onto dye degradation under solar light for 60 min duration after attaining adsorption-desorption equilibrium for each individual ZnO powder. Each of the photocatalytic experiment has been carried at a constant catalyst loading of 50 mg/L, at room temperature of 25 ± 2 ^{o}C, pH ~ 6, visible light intensity of 42800 lux and average solar intensity 0.768 kW m^{-2}. Prior to the experiments,

View Article Online
DOI: 10.1039/C6RA10472J

degradation of the dye was studied in the pH range between 3 and 11. The lower pH was avoided as crystal violet undergoes color change at pH < 2. The initial pH was adjusted by adding 1 N HNO_3 or 1 N NaOH. It was observed that the dye degradation was not much influenced by pH and the variation observed was only 2-3% by the change of pH. However, at pH higher than 6, dye solution affected the UV-Vis spectra. Thus, all the experiments were conducted at pH ~ 6. The calculated degradation percentage has been plotted as histogram and shown in Figure 8a. It was observed that spongy-ZnO synthesized by citric acid shows better photodegradation of 89% in comparison to other quasi-fiber (oxalic acid) and flake (urea) morphology that imparts only 67% and 46% degradation, respectively in 60 min duration. It is evident from surface area data (section 3.3) that flake like structure and quasi-fiber should show less degradation. The decrease in degradation can be attributed probably to low surface area and high agglomeration of particles that reduces number of active sites for interaction during the catalytic reaction. Thus, it can be accredited that porous structure and high surface area of sponge like zinc oxide provides the open pore channel for active sites to react and enhance the photochemical process. Since, spongy-ZnO synthesized using citric acid showed highest activity under solar light. Therefore, detailed degradation profile and kinetics were studied only for this catalyst.

Porous catalysts are promising for practical applications. The photolysis and degradation profile of CV dye with respect to time in the presence of a catalyst spongy-ZnO under various conditions has been shown in Figure 8b. The profile is plotted as the variation of C/C_o with time where, C is the concentration of the CV at different time and C_o is the initial concentration of the CV dye. Initially, photolysis was carried in the presence of the visible light to understand the effect of light on the CV dye. Approximately, 10% of the dye was degraded in the individual presence of light without any catalyst. Each photocatalysis experiment has been carried using optimized spongy-ZnO catalyst. The photocatalysis experiments have been carried after adsorption-desorption equilibrium under a dark condition in the presence of ZnO catalyst. There is not much difference between the photolysis and adsorption of the dye onto the spongy-ZnO catalyst. Since the surface of ZnO is

View Article Online
DOI: 10.1039/C6RA10472J

positively charged, therefore, negatively charged dye molecules easily adsorbs onto the surface but only 11% of the dye is adsorbed in 1 h [27]. Spongy-ZnO has been used for photocatalytic degradation of CV under the influence of visible light and naturally occurring solar light. The photodegradation of CV is 78% in the presence of visible light. However, 89% degradation is observed in the presence of solar light. The enhanced catalytic degradation can be attributed to the active surface sites available due to the porous nature of the spongy-ZnO and high surface area. This could also be the influence of solar light as the natural solar light has nearly 4% of UV light and ZnO is an UV active material. In order to further evaluate the photoactivity of prepared spongy-ZnO, degradation of CV in the presence of commercially available Degussa P-25 TiO_2 was also performed under the influence of solar light. The degradation of CV was only 49% in 1 h, which is very less in comparison to the prepared catalyst under both visible and solar light. It can be attributed that porous structure and rough surface promotes the degradation process. In recent past, ZnO nanoflowers were prepared by a simple solution method to degrade CV dye [26]. Under UV light illumination, 96% CV was degraded in 80 min but in the present case 89 % CV dye degrades under solar light which makes porous spongy zinc oxide a superior material.

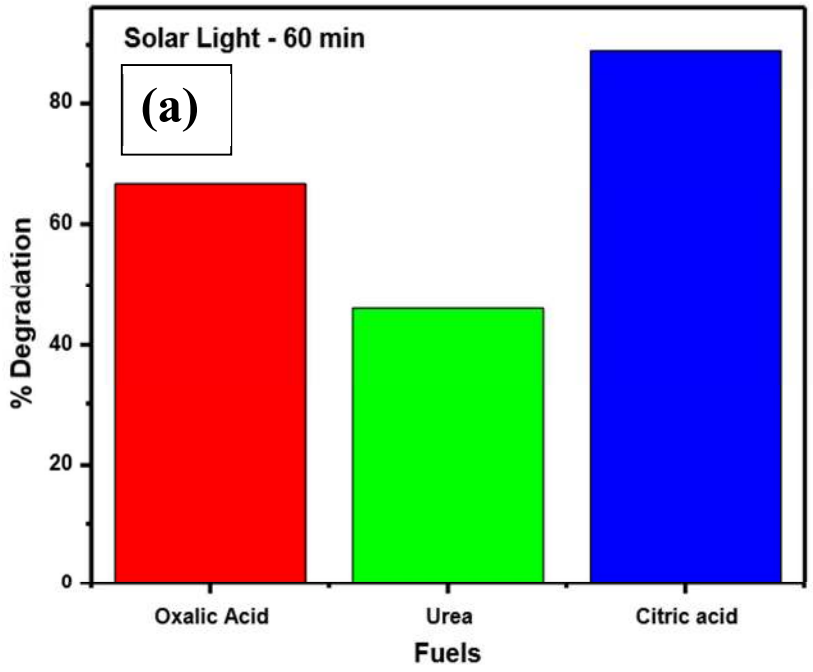

View Article Online
DOI: 10.1039/C6RA10472J

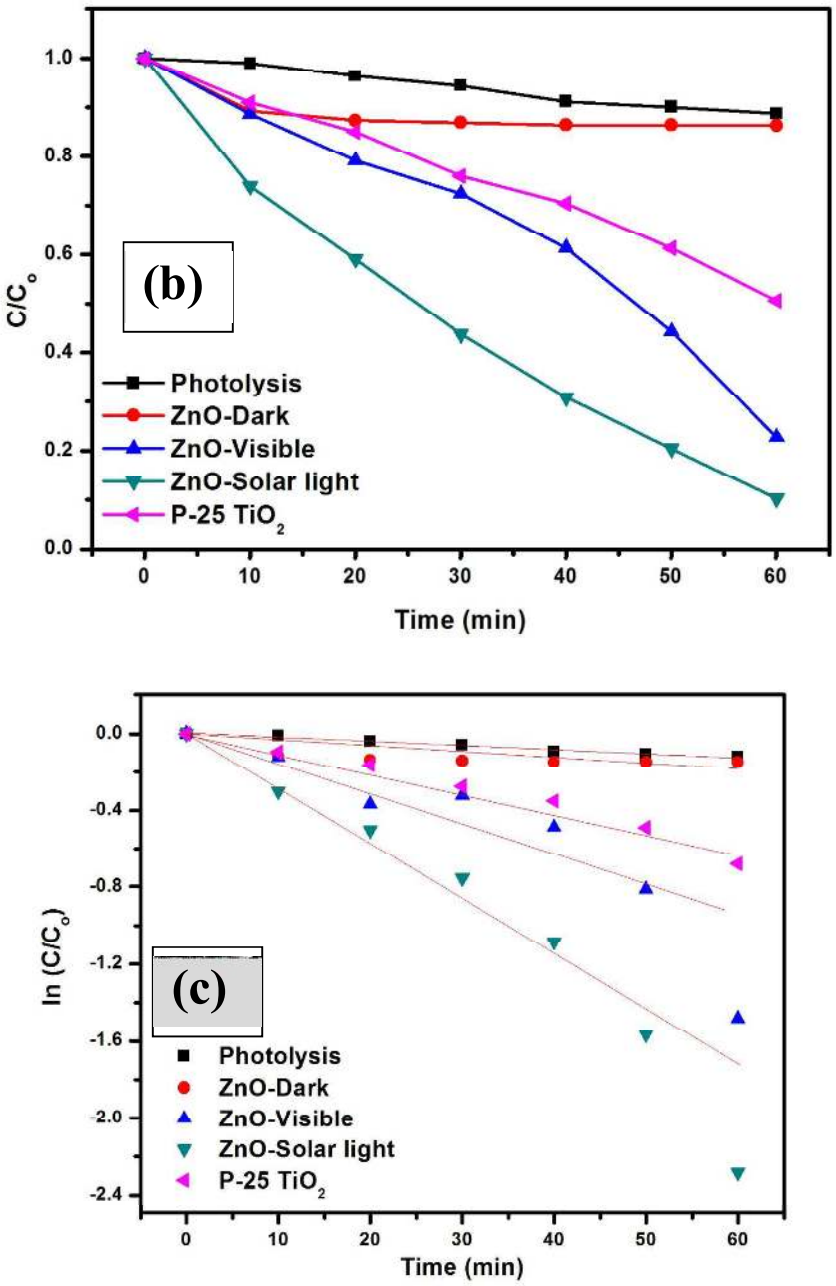

Figure 8: (a) Photocatalytic degradation using different fuels, (b) Photocatalytic degradation profile and (c) kinetic profile of Crystal Violet dye (Initial dye concentration = 20 mg L^{-1}, catalyst loading = 50 mg L^{-1}, temperature = 25 ± 2^{o}C, pH ~ 6, visible light intensity = 42800 lux, and solar intensity = 0.768 kW m^{-2})

In order to investigate whether the photochemical reaction follows pseudo-first order kinetics, ln (C/C_o) was plotted with time for photolysis, dark-adsorption, and catalysis experiments. Figure 8c shows the kinetic profiles and the kinetic rate constant k was obtained from the slope of this plot. The

View Article Online
DOI: 10.1039/C6RA10472J

kinetic rate constant of spongy-ZnO is 0.035 min^{-1} which is three times higher than that of rate constant (0.011 min^{-1}) of P-25 TiO_2 catalyst. On the other hand, the calculated kinetic rate constant of visible light irradiated spongy-ZnO is 0.021 min^{-1}, which is comparatively lower than solar light irradiated photochemical reaction. Further increment can be expected in presence of UV light solely, as ZnO is highly UV active. However, the results entail that the spongy-ZnO effectively degrades CV and is a better photocatalyst in comparison to Degussa P-25 TiO_2 in the presence of solar light.

3.7. Reusability and Reaction Mechanism

In all the environmental remedial processes, reusability of the material is a key parameter. Although, research has been carried on the catalytic performance of ZnO and ZnO based materials, but reliability and reusability mechanism are limited. In the present work, the performance of the spongy-ZnO on consecutive recycling under the influence of visible light and solar light was evaluated and shown in Figure 9a and Figure 9b, respectively. In the presence of visible light (Figure 9a), no significant change in the degradation was observed for five consecutive cycles and the degradation % decreased from 78% to 75% after five cycles indicating nearly stable activity. A constant decreasing trend was observed in the presence of solar light (Figure 9b). The photodegradation percentages for 1^{st}, 2^{nd}, 3^{rd}, 4^{th} and 5^{th} cycle are 89%, 87%, 86%, 84.7% and 83%, respectively. This decrease in trend could be attributed to the photocorrosion (Eq. 2) and also photoinduced dissolution occurring on the surface of ZnO due to the presence of 4% UV light in the total sunlight. The reason for photocorrosion is the hole participation that destroys the structure of ZnO.

$$ZnO + 2h^+ + nH_2O \rightarrow Zn(OH)_n^{2-n} + 1/2\ O_2 + nH^+ \quad (2)$$

In recent past, ZnO nanocrystals were found to have superior photocatalytic and antiphotocorrosion property than commercial ZnO [28]. Thus, solar light experiments were carried to compare the photocorrosion property of commercial ZnO for five consecutive cycles. Photodegradation by commercial ZnO was 60 % after first run which reduced by 14% after 5

View Article Online
DOI: 10.1039/C6RA10472J

consecutive cycles whereas Spongy-ZnO shows maximum catalytic efficiency even after five cycles with a difference of only 6%.

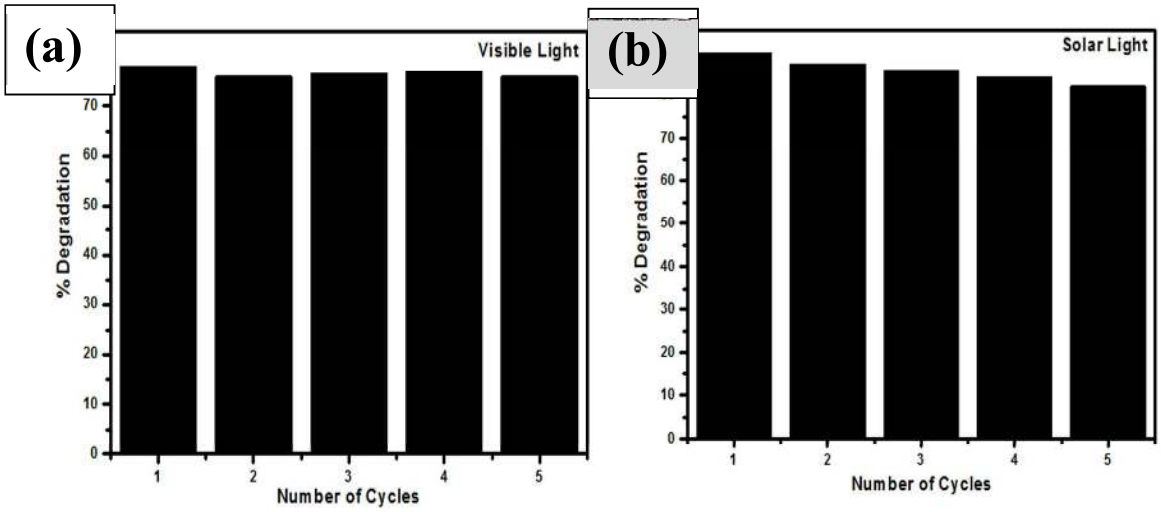

Figure 9: Reuse of the photocatalyst under (a) Visible light and (b) Solar light. (Initial dye concentration = 20 mg L^{-1}, catalyst loading = 50 mg L^{-1}, temperature = 25 ± 2°C, pH ~6, visible light intensity = 42800 lux, and solar intensity = 0.768 kW m^{-2})

The rate of photocatalytic degradation is directly proportional to the amount of reactive oxidative species (ROS) generated as a result of generation of electron-hole pairs upon irradiation of photon energy. The degradation rate is influenced by the presence of electron acceptors such as oxygen or hydrogen peroxide. These electron acceptors enhance the rate of degradation by inhibiting the recombination of electron-hole pair by accepting the electron in conduction band and also increase the concentration of hydroxyl radicals for enhanced photocatalytic activity [29]. The photocatalytic degradation of CV under solar light was studied at different concentrations of H_2O_2 in the presence of catalyst and without catalyst as shown in Figure S1 (Supplementary information).

The rate of degradation increases with increasing concentration of H_2O_2 but the degradation rate does not increase beyond 2 mM concentration. The result suggests that the lower concentration of hydrogen peroxide effectively produces enough hydroxyl radicals that inhibit the electron-hole recombination enhancing the photodegradation as shown in Eq. 3 and Eq. 4. At high H_2O_2 concentration under solar light, hydrogen peroxide itself reacts with hydroxyl radicals to produce

View Article Online
DOI: 10.1039/C6RA10472J

perhydroxyl radicals, which is a weak oxidant compared to hydroxyl radicals [30] as shown in Eqs. 5 and 6. Therefore, an optimum amount of H_2O_2 is needed for effective photodegradation of CV and addition of excess H_2O_2 has no significant effect on the degradation.

$$e_{CB}^{-} + H_2O_2 \rightarrow OH^{-} + \cdot OH \quad (3)$$

$$H_2O_2 + h\upsilon \rightarrow 2 \cdot OH \quad (4)$$

$$H_2O_2 + \cdot OH \rightarrow H_2O + OH_2 \cdot \quad (5)$$

$$H_2O_2 + h_{VB}^{+} \rightarrow H^{+} + OH_2 \cdot \quad (6)$$

Figure 10 shows the schematic detailing the mechanism for photodegradation of CV in the presence of spongy-ZnO that explains the transfer of photogenerated electrons and holes to the surface of the photocatalyst to react with H_2O and O_2 to generate $\cdot O_2^-$ and ·OH radicals as ROS. The oxidation of pollutant occurs in the presence of radicals due to their high oxidation capacity [31]. In order to better understand the involvement of electron or hole species in the photochemical degradation of crystal violet under solar light, several scavenging experiments were systematically carried in support of the photocatalytic mechanism. The trapping agents used were benzoquinone (BQ), tertiary butyl alcohol (t-BuOH), dimethylsulphoxide (DMSO) and EDTA-2Na for scavenging $\cdot O_2^-$ radical, ·OH radical, electron and hole, respectively.

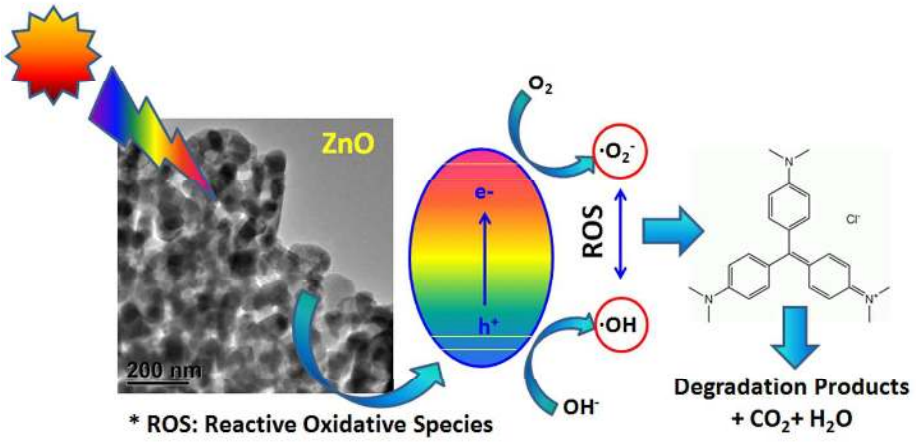

Figure 10: Schematic mechanism of ZnO as photocatalyst.

View Article Online
DOI: 10.1039/C6RA10472J

Prior to the scavenging experiments, control experiments were performed in the presence of spongy-ZnO catalyst only. Figure 11(a) shows the experimental plot of degradation profile with respect to time and Figure 11(b) presents the plot of rate constants calculated for different scavengers. The plot shows that the rate constant in the presence of t-BuOH is reduced which suggests that hydroxyl radicals are trapped during the reaction such that reaction is hindered to proceed for further photochemical reaction. The presence of DMSO has no influence on the photochemical reaction and the degradation reaction rate constant is equivalent to the control experiment. This confirms that the prime reactive oxidative species in the present study is the ˙OH radicals. However, the presence of EDTA-2Na results in a degradation rate constant of 0.024 min^{-1} while that obtained in the presence of t-BuOH is 0.015 min^{-1}. This suggests that both t-BuOH and EDTA-2Na are effectively trapping the ·OH radicals and holes, respectively. The presence of both of these scavengers influences the dye degradation compared to the other scavengers present in the system. The above results show that the holes and surface hydroxyl radicals play a significant role in the photocatalytic degradation of CV dye under solar light. Thus, combustion synthesized spongy-ZnO powders can act as a promising photocatalyst due to its effective performance under both visible and solar light with good recycling performance.

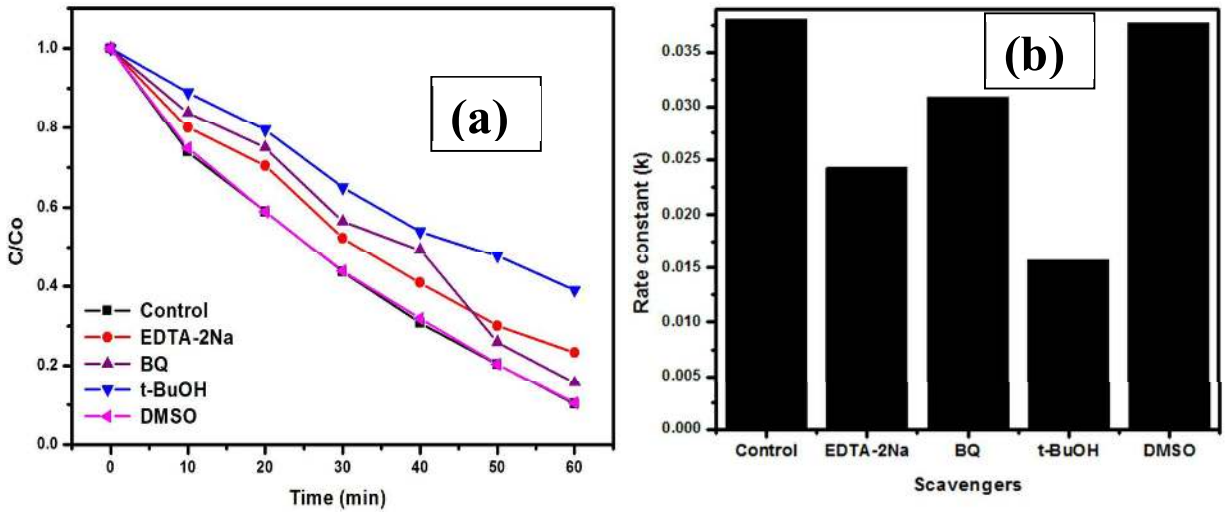

Figure 11: (a) Degradation profile and (b) rate constant under influence of different scavengers. (Initial dye concentration = 20 mg L^{-1}, catalyst loading = 50 mg L^{-1}, temperature = 25 ± 2°C, pH ~6, and solar intensity = 0.768 kW m^{-2})

View Article Online
DOI: 10.1039/C6RA10472J

3.8. Effect of ZnO on *E.coli* bacterium

Figure 12 shows the degradation profile of *E.coli* under photolysis, ZnO and commercial Degussa P-25 TiO_2. For all the inactivation reactions, pseudo-first order kinetic was observed. The first order rate of inactivation of bacteria is given by [32]

$$\ln\left(\frac{C_c}{C_{C_0}}\right) = -\mathrm{k}'\mathrm{t} \qquad (7)$$

In Eq. (7), k′ is rate constant, C_{C_0} is initial cell concentration (CFU/mL), C_c is the cell concentration (CFU/mL) at t time (h). The rate constants were evaluated by linear regression. k' are tabulated in Table 1. Pseudo first order inactivation kinetics was followed [33, 34] in all cases (Figure S2).

The dramatic enhancement in photocatalytic activity was observed by using photocatalyst ZnO under visible light irradiation compared to Degussa P-25 TiO_2. The surface area of TiO2 is 50 m^2/g. High surface area and porous sponge-like morphology (section 3.3) of the photocatalyst suggested that there is high interaction possibility of bacteria with the material. Electrons in conduction band reacts with the electron acceptor species and forms superoxide radicals and holes located at valence band react with electron donor species and form hydroxyl radicals. The radical formation leads to the killing of bacteria by rupturing the cell membrane /cytoplasmic membrane [35, 36] which allows active penetration of these generated reactive oxygen species / radicals (ROS) into the membrane. Photoelectrochemical oxidation of CoA (Coenzyme A) is responsible towards inactivation of bacteria. This inhibits the respiratory mechanism of bacterium causing disturbance in the metabolic activity of which leads to cell death [37, 38]. Efficient charge separation also increases the photo-inactivation activity. The reduced band gap (2.92 eV) of the material results in absorption of longer wavelength light [37] that enhance the visible light activity of the spongy-ZnO.

View Article Online
DOI: 10.1039/C6RA10472J

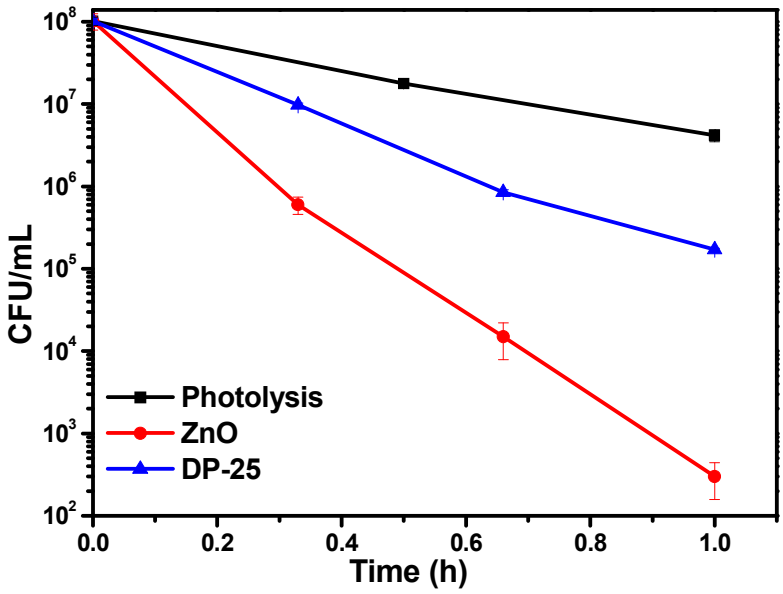

Figure 12. Degradation profile of E. coli under visible irradiation for photolysis, spongy-ZnO and P-25 TiO_2. (Initial concentration ~10^8 CFU/ml, catalyst loading = 0.25 g/L, temperature = 25 ± 2°C, and visible light intensity = 42800 lux)

3.9. Effect of H_2O_2 addition on *E.coli*

Hydroxyl radical (ȮH) plays a very important role in inactivation of the bacteria by oxidation of the microbial or inorganic contamination as described above. Hydroxyl radical (ȮH) is generated as a result of dissociation of H_2O_2 [39]. Formation of H_2O_2 occurs as an intermediate in the reaction mechanism as follows (Eq.8-13):

$$ZnO \xrightarrow{h\theta \geq \text{band gap}} h^+(V.B.) + e^-(C.B.) \quad (8)$$

$$OH^- + h^+ \rightarrow \dot{O}H \quad (9)$$

$$O_2 + e^- \rightarrow O_2^{\dot{-}} \quad (10)$$

$$2O_2^{\dot{-}} + 2H^+ \rightarrow H_2O_2 + O_2 \quad (11)$$

$$H_2O_2 \rightarrow 2\dot{O}H \quad (12)$$

$$h^+(V.B.) + e^-(C.B.) \xrightarrow{k_{recombination}} \text{heat} \quad (13)$$

View Article Online
DOI: 10.1039/C6RA10472J

Figure S3 shows the degradation profile after addition of H_2O_2 with the ZnO photocatalyst. In order to generate ROS in the solution by photocatalyst, addition of 2, 10, 100, 250 and 500 mM H_2O_2 was done to provide accelerated ROS radicals externally [33]. A low concentration of 2 mM of H_2O_2 addition does not affect the inactivation rate of bacteria. However, as concentration of H_2O_2 is increased from 2 mM to 10 mM, the inactivation rate increases gradually. A drastic increase in inactivation rate is observed as the concentration of H_2O_2 increased from 10 mM to 100 mM. The results depict that only 20 min is sufficient to degrade the bacteria by 7-log reduction in bacterial count. Hydrogen peroxide dissociates to generate hydroxyl and superoxide radicals at faster rate and equation following the process has been mentioned in section 3.6 (Eq 3-6). It was suggested that addition of H_2O_2 accelerates the reduction of electrons present on conduction band and also it consumes the holes present on the valence band in oxidation reaction which suppresses the recombination [40].

Table 1. Rate constants of photocatalysis degradation of *E.coli* under visible light irradiation.

Photocatalysts (Visible)	**Rate constants [h^{-1}]**
Photolysis	3.25 ± 0.08
ZnO	13.11 ± 0.4
DP-25	6.68 ± 0.2
2 mM H_2O_2 + ZnO	13.73 ± 0.3
10 mM H_2O_2 + ZnO	15.94 ± 0.8
100 mM H_2O_2 + ZnO	49.54
250 mM H_2O_2 + ZnO	51.09
500 mM H_2O_2 + ZnO	52.20

Figure S4 shows the kinetics followed in inactivation reaction of *E.coli*. The rate constant k' varies with the concentration of H_2O_2 as shown in Figure S5. It follows a form, $k' = k_1 C_H/(1 + k_2 C_H)$ where C_H is concentration of H_2O_2. Thus, a plot of k'/C_H with C_H is expected to be linear as shown in inset of Figure S5. The rate constant values presented in Table 1 shows that there has been a

View Article Online
DOI: 10.1039/C6RA10472J

drastic change from 10 mM to 100 mM H_2O_2 addition. However, further increase in H_2O_2 concentration does not have any significant effect towards bacterial inactivity. Thus, the result depicts that 100 mM H_2O_2 is sufficient for bacterial inactivation.

4. CONCLUSIONS

Porous spongy-ZnO photocatalyst were synthesized via easy, cost-effective and one step solution combustion method under stoichiometric oxidizer to fuel ratio at temperature 400^{o}C in 40 min time duration. Photocatalysis inactivation demonstrated 6-log reduction in bacterial enumeration in 1 h. Visible light irradiation degrades approximately 80% of the crystal violet dye whereas 90% of the organic pollutant is degraded in the presence of spongy-ZnO photocatalyst under the naturally occurring solar light. The superiority in photodegradation could be attributed to combined effect of both UV and visible light. The as-synthesized ZnO shows superior photoactivity with effective recycling performance till five cycles without any significant decrease in catalytic efficiency. An optimum of 2 mM H_2O_2 concentration exhibits effective photodegradation of organic pollutant but 100 mM H_2O_2 with 0.25 g/L ZnO showed 7-log reduction in *E.coli* count in just 20 min. Both the photocatalytic degradation and photo-conversion efficiency has enhanced due to effective separation of recombination pairs. Spongy-ZnO has high catalytic potential in environmental based waste water purification and also bacterial inactivation. Our process is imperative for potential application of ZnO material because of the simple synthesis method, low cost, large scale production with excellent photochemical performance under visible light.

Acknowledgements

Dr. Sangeeta Adhikari would like to thank UGC-Dr. D. S. Kothari Postdoctoral Fellowship scheme and the corresponding author thanks the Department of Science and Technology, Government of India for the J.C. Bose fellowship.

Supporting information

Some figures are shown in supporting information.

References:

View Article Online
DOI: 10.1039/C6RA10472J

[1] M. R. Hoffmann, S. T. Martin, W. Y. Choi and D. W. Bahnemann, *Chem. Rev.,* 1995, **95**, 69-96.

[2] M. L. Curri, R. Comparelli, P. D. Cozzoli, G. Mascolo and A. Agostiano, *Mater. Sci. Engg. C*, 2003, **23**, 285-289.

[3] Y. Ni, X. Cao, G. Wu, G. Hu, Z. Yang and X. Wei, *Nanotechnology*, 2007, **18**, 155603-155608.

[4] A. J. Hoffman, E. R. Carraway and M. R. Hoffmann, *Environ. Sci.Technol.,* 1994, **28**, 776-785.

[5] X. Chen and S. S. Mao, *Chem. Rev.*, 2007, **107**, 2891-2959.

[6] Y. Zhang, M. K. Ram, E. K. Stefanakos and D. Y. Goswami, *J. Nanomater.*, 2012, **2012**, 1-22.

[7] R. Nagaraja, N. Kottam, C. R. Girija and B. M. Nagabhushana, *Pow. Technol*., 2012, **215**, 91-97.

[8] A. J. Reddy, M. K. Kokila, H. Nagabhushana, J. L. Rao, C. Shivakumara, B. M. Nagabhushana and R. P. S. Chakradhar, *Spectrochim. Acta Part A*, 2011, **1**, 53-58.

[9] C. S. Lin, C. C. Hwang, W. H. Lee and W. Y. Tong, *Mater. Sci.Eng., B*, 2007, **140**, 31-37.

[10] A. Mclaren, T. V. Solis, G. Li and S. C. J. Tsang, *Am. Chem. Soc.*, 2009, **131**, 12540-12541.

[11] P. R. Potti and V. C. Srivastava, *Ind. Eng. Chem. Res.*, 2012, **51**, 7948–7956..

[12] M. A. Ali, M. R. Idris and M. E. Quayum, *J. Nanostructure in Chem.*, 2013, **3**, 36-42.

[13] T. Jansson, Z. J. Clare-Salzler, T. D. Zaveri, S. Mehta, N. V. Dolgova, B.-H. Chu, F. Ren and B. G. Keselowsky, *J. Nanosci. Nanotechnol.*, 2012, **12**, 7132–7138.

[14] R. S. Subhasree, D. Selvakumar and N. S. Kumar, *Lett. in Appl. NanoBioScience*, 2012, **1**, 2–7.

[15] T. V. Anuradha and S. Ranganathan, *Bull. Mater. Sci.*, 2007, **30**, 263-269.

[16] N. Riahi-Noori, R. Sarraf-Mamoory, P. Alizadeh and A. Mehdikhani, *J. Ceram. Processing Res.*, 2008, **9**, 246-249.

[17] L. Conceicao, A. M. Silva, N. F. P. Ribeiro and M. V. V. M. Souza, *Mater. Res. Bull.*, 2011, **46**, 308-314.

[18] N. Rajamanickam, R. N. Mariammal, S. Rajashabala and K. Ramachandran, *J. Alloys Compd.*, 2014, **614**, 151-164.

[19] G. Zhang, X. Shen and Y. Yang, *J. Phys. Chem. C*, 2011, **115**, 7145-7152.

View Article Online
DOI: 10.1039/C6RA10472J

[20] Y. Cao, B. Liu, R. Huang, Z. Xia and S. Ge, *Mater. Lett.*, 2011, **65**, 160-163.

[21] P. Cai, D. Zhen, X. Xu, Y. Liu, N. Chen, G. Wei and A. Sui, *Mater. Sci. Eng. B,* 2010, **17**, 116-119.

[22] L. Song, S. Zhang, X. Wu and Q. Wei, *Ind. Eng. Chem. Res.*, 2012, **51**, 4922-4926.

[23] S. Sarkar, A. Makhal, T. Bora, S. Baruah, J. Dutta and S. K. Pal, *Phys. Chem. Chem. Phys*., 2011, **13**, 12488-12496.

[24] A. V. Dijken, E. A. Meulenkamp, D. Vanmaekelbergh and A. Meijerink, *J. Phys. Chem. B*, 2000, **104**, 1715-1723.

[25] J. Lee, H. S. Shim, M. Lee, J. K. Song and D. Lee, *J. Phys. Chem. Lett.*, 2011, **2**, 2840-2845.

[26] S. Ameen, M. S. Akhtar, M. Nazim and H. S. Shin, *Mater. Lett*. , 2013, **96**, 228-232.

[27] K. M. Kim, M. H. Choi, J. K. Lee, J. Jeong, Y. R. Kim, M. K. Kim, S. M. Paek and J. M. Oh, *Int. J. Nanomedicine*, 2014, **9**, 41-56.

[28] R. Velmurugan, K. Selvam, B. Krishnakumar and M. Swaminathan, *Separation and Purification Technol.,* 2011, **80**, 119-124.

[29] B. Li and H. Cao, *J. Mater. Chem.*, 2011, **21**, 3346-3349.

[30] D. H. Tseng, L. C. Juang and H. H. Huang, *Int. J. Photoenergy*, 2012, 1-9.

[31] J. Zhou, M. Zhang and Y. Zhu, *Phys. Chem. Chem. Phys.*, 2014, **16**, 17627-17633.

[32] L. L. Gyürék and G.R. Finch, *J. Environ. Engg*., 1998, **124**, 783-793.

[33] S. Sontakke, C. Mohan, J. Modak and G. Madras, *Chem. Eng. J.*, 2012, **189**, 101-107.

[34] J. Ren, W. Wang, L. Zhang, J. Chang and S. Hu, *Catal. Comm.*, 2009, **10**, 1940-1943.

[35] K. Sunada, T. Watanabe and K. Hashimoto, *J. Photochem. & Photobio. A: Chem.*, 2003, **156**, 227-233.

[36] M. Wu, T. Bak, P. O'Doherty, M. Moffitt, J. Nowotny, T. Bailey and C. Kersaitis, *Int. J. Photochem*., 2014, **2014**, 1-9.

[37] T. Matsunaga, R. Tomoda, T. Nakajima and H. Wake, *FEMS Microbiology Lett.*, 1985, **29**, 211-214.

View Article Online
DOI: 10.1039/C6RA10472J

[38] S. Sontakke, J. Modak and G. Madras, *Chem. Eng. J.*, 2010, **165**, 225-233.

[39] S. Sontakke, J. Modak and G. Madras, *Appl. Catal. B: Environ.*, 2011, **106**, 453-459.

[40] T. Hirakawa and Y. Nosaka, *Langmuir*, 2002,**18**, 3247-3254.

View Article Online
DOI: 10.1039/C6RA10472J

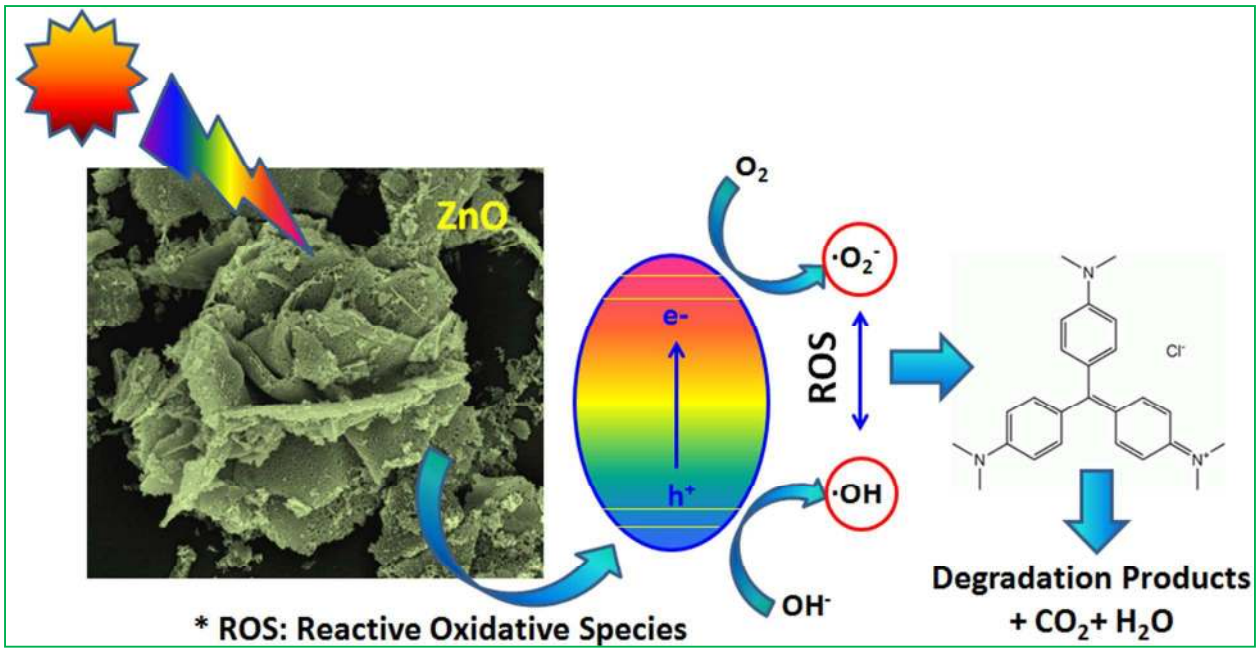

Citric acid assisted spongy-ZnO nanopowders exhibit high catalytic activity for dye degradation and towards bacterial inactivation.